# Uncertainty analysis of satellite rainfall input data in a hydrological model using the Generalized Likelihood Uncertainty Estimation (GLUE) method

*Hendry* Rinduan[1], *Hero* Marhaento[1*], *Ambar* Kusumandari[1], *Hatma* Suryatmojo[1], *Muhammad Chrisna* Satriagasa[1], and *Winggar Cahyo* Andhika[1]

[1]Forest Resources Conservation Dept., Faculty of Forestry, Universitas Gadjah Mada, Yogyakarta 55281, Indonesia

**Abstract.** Uncertainty analysis estimates the range of variability in a model's expected results. A main source of uncertainty in hydrological models is rainfall input data. This study aims to evaluate the uncertainty in satellite-based rainfall data for the *Hydrologiska Byråns Vattenbalansavdelning* (HBV) hydrological model using the Generalized Likelihood Uncertainty Estimation (GLUE) method. The Upper Bogowonto Watershed, Central Java, is selected to test the method. The results of the study showed that bias correction significantly reduced the bias in satellite rainfall data. The reference model using field observation data demonstrated good performance, with $R^2 = 0.64$ and KGE = 0.80 for the calibration period and $R^2 = 0.63$ and KGE = 0.78 for the validation period. The GLUE analysis revealed that the range of input data uncertainty covered 60% of the observation data during the calibration period and 63% during the validation period. High uncertainty occurred during peak flow and tended to be lower during low flow. The GSMaP satellite data were considered the best rainfall input data for the hydrological model in the Upper Bogowonto Watershed.

## 1 Introduction

Hydrology, derived from the Greek words 'Hydro' (water) and 'Logia' (study), is the science that examines water in all its forms liquid, gas, and solid on, above, and below the Earth's surface. It focuses on the distribution, properties, cycles, and interactions of water with living organisms [1]. The hydrological cycle, which involves processes such as precipitation, condensation, transpiration, and evapotranspiration, is central to understanding water dynamics [1]. With the accelerating impacts of climate change, hydrological studies have become increasingly critical for water and soil conservation, erosion control, and understanding the relationship between rainfall, runoff, and watershed characteristics [1]. These studies are also essential for regional and national water management planning, weather forecasting, and sustainable development.

* Corresponding author: marhaento@ugm.ac.id

Hydrological models are indispensable tools for simulating water movement and behavior. They simplify complex natural processes, aiding in decision-making and planning. Among these models, the *Hydrologiska Byråns Vattenbalansavdelning* (HBV) model, a semi-distributed conceptual model, is widely used [2]. However, hydrological models are inherently limited by uncertainties arising from data availability, measurement accuracy, and the simplification of real-world conditions [3]. These uncertainties can significantly impact model reliability, making it crucial to understand and communicate them effectively.

Rainfall data is a critical input for hydrological models, driving responses such as runoff and peak discharge in watersheds [2]. However, in regions like Indonesia, high spatial and temporal variability in rainfall poses significant challenges for accurate prediction and water management. Traditional ground-based observations often suffer from incomplete data, uneven station distribution, and manual collection systems. Satellite-derived rainfall data, such as CHIRPS, TRMM, GPM, PERSIANN, and CPC, offer a promising alternative with improved spatial and temporal resolutions [4].

This study evaluates the suitability of various satellite-derived rainfall datasets for hydrological modeling using the HBV model. By comparing these datasets, we aim to identify the most reliable source for hydrological analysis, thereby supporting better water resource management decisions. The research focuses on the Upper Bogowonto Watershed, selected for its high-quality observational data, which provides a robust basis for validating satellite-derived rainfall estimates and assessing model uncertainty.

## 2 Materials and Methods

### 2.1 Study Area

This study was conducted in the Upper Bogowonto Watershed, located between 7°23'02.34" S – 7°42'14.30" S latitude and 110°01'56.43" E – 110°04'18.97" E longitude. The research area spans four regencies in Central Java Province and the Special Region of Yogyakarta, Indonesia, including Wonosobo Regency (northwest), Magelang Regency (east), Purworejo Regency (south), and a small area of Gunungkidul Regency (south). Data collection and analysis were carried out from October to November 2024.

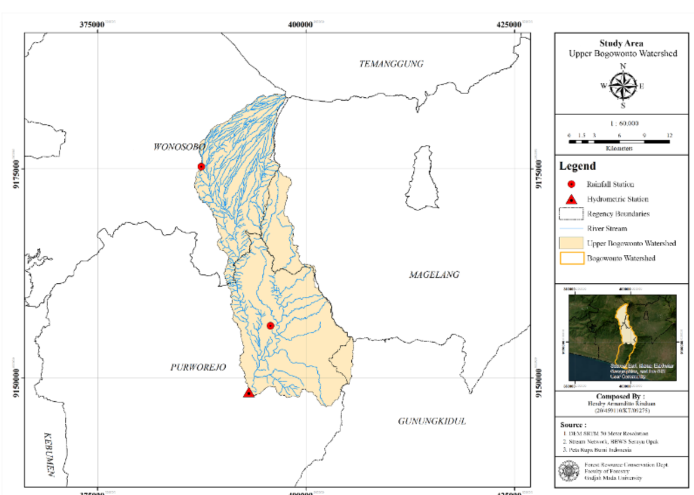


**Fig. 1.** Elevation zone categories [5]

## 2.2 Data Collection

### *2.2.1 Topographic data*

The Digital Elevation Model (DEM) used in this study was derived from the Shuttle Radar Topography Mission (SRTM), a NASA satellite initiative that provides global topographic data at a spatial resolution of 1 arc-second (~30 meters). SRTM was selected due to its high spatial resolution, global coverage (including 80% of Earth's surface), and accessibility for spatial analyses. This DEM was critical for defining elevation zones in the HBV model setup. The SRTM DEM was processed in ArcGIS to refine its applicability to the study area, where a reclassification analysis was performed to categorize slope classes based on classification rules.

**Table 1.** Elevation zone categories [5]

| Elevation Zone | Elevation (mdpl) |
|---|---|
| 1 | <10 |
| 2 | 10 - 50 |
| 3 | 100 - 500 |
| 4 | 500 - 1000 |
| 5 | 1000 - 15000 |
| 6 | >1500 |

### *2.2.2 Climate data*

The required climate data include temperature, potential evapotranspiration (PET), and precipitation. Temperature data were obtained from the Serayu Opak River Basin Authority (BBWSSO), a governmental hydrological institution. Potential evapotranspiration was calculated using the Hargreaves-Samani method, selected due to the limited availability of climatic variables in the study area. This method is widely recognized for its ability to estimate PET with minimal input requirements, relying solely on air temperature data [6], making it suitable for regions with constrained meteorological datasets.
The equation used is as follows:

$$\mathrm{ETP} = 0.0023 \text{ x } R_A \text{ x } TD^{0.5}(TC^{\circ}+17.8) \tag{1}$$

where ETP is the potential evapotranspiration, $R_A$ is the extraterrestrial radiation, TD is the difference between maximum and minimum temperature, and TC is the average temperature Extraterrestrial radiation can be calculated using the formula:

$$\mathrm{R_A} = \frac{24(60)}{\pi} \text{ x } G_{SC} \text{ x } d_r[\omega_s \sin(\varphi)\sin(\delta)\sin(\omega_s)] \tag{2}$$

$$\delta = 0.409\sin(\frac{2\pi \mathrm{J}}{365} - 1.39) \tag{3}$$

where GSC is the constant solar radiation (0.0820 MJ m-2 min-1), dr is the Inverse of the Earth to sun distance, J is the day of the year, ωs is the sunset hour angle (radians), φ is the point of latitude (radian), and δ is the sun declination angle (radians)

Two types of rainfall data were utilized: observational rainfall data and satellite-derived rainfall data. Daily rainfall records spanning 2012–2018 were acquired from the Serayu Opak River Basin Authority (BBWS Serayu Opak) for observational data and the Google Earth Engine database for satellite data. Observational rainfall data were collected from individual gauge stations, while satellite data provided spatially distributed estimates.

Since the HBV hydrological model requires area-averaged rainfall inputs, the Thiessen polygon method was applied to compute spatially weighted mean rainfall across the study area. Using ArcGIS software, Thiessen polygons were generated to delineate the influence zones of each rain gauge station. The daily areal rainfall (*P*) was calculated as:

$$\underline{P} = \frac{\sum A_n P_n}{A} \tag{4}$$

where *An* represents the influence area of station n, *Pn* is the rainfall recorded at station n, and *A* is the total study area.

**Table 2.** Description of satellite data used in this study

| Dataset | Developer | Temporal Resolution | Temporal Coverage |
|---|---|---|---|
| **CHIRPS** | CHG | Daily | 1981 - 2024 |
| **TRMM 3B42** | NASA dan JAXA | 3 h | 1998 - 2019 |
| **GPM v8** | NASA dan JAXA | 30 min | 2000 - 2004 |
| **PERSIANN-CDR** | CHRS | Daily | 1983- 2024 |
| **GSMaP v8** | JAXA | 1h | 1998 - 2024 |
| **ERA5-Land** | ECMWF | Daily | 1950 - 2024 |
| **CPC** | NOAA | Daily | 2006 - 2024 |

## 2.3 Bias Correction

Before further analysis, bias correction was applied to the satellite-derived rainfall data to address systematic errors influenced by elevation, latitude, climatic conditions, and precipitation mechanisms. The Quantile Mapping (QM) method was employed, which statistically aligns the satellite data with ground-based observations to reconcile scale discrepancies between the two datasets [7]. The correction was implemented using the *qmap* package in R software, a widely recognized tool for non-parametric distribution mapping.

The equation used is as follows:

$$Po=Fo^{-1}(Fm(Pm)) \quad (5)$$

Where Po is the observed data, Fo-1 is the inverse CDF of observed rainfall data, Fm is the Cumulative Distribution Function (CDF), and Pm is the simulated rainfall data (satellite rainfall data).

The bias-corrected satellite rainfall data were quantitatively assessed using the Percent Bias (PBIAS) metric to evaluate improvements relative to the original uncorrected dataset. PBIAS measures the average tendency of satellite estimates to deviate from observational data and is calculated as:

$$PBIAS(\%)=\frac{\sum_{i=1}^{n}(Q_o\text{-}Q_s)_i}{\sum_{i=1}^{n}Q_o} \text{ x } 100 \quad (6)$$

where $Q_S$ and $Q_O$ represent the satellite-derived and observed rainfall values, respectively, for N paired data points.

**Table 3.** Performance Rating for PBIAS [8]

| Performance Rating | PBIAS |
|---|---|
| Very Good | PBIAS ≤ ±10 |
| Good | ±10 < PBIAS ≤ ±15 |
| Satisfactory | ±15 < PBIAS ≤ ±25 |
| Unsatisfactory | PBIAS ≥ ±25 |

## 2.4 Modelling Process

### *2.4.1 Model setup*

The dataset was partitioned into warm-up (2012), calibration (2013–2016), and validation (2017–2018) periods in a 1 : 4 : 2 ratio. Observed rainfall served as the reference dataset to establish the HBV-Light hydrological model, which was subsequently driven by satellite-based rainfall products to evaluate their reliability. Daily inputs included potential evapotranspiration, temperature, and rainfall, formatted to meet software requirements. Initial model parameters (e.g., FC, LP, BETA for soil routines; PERC, UZL, $K_0$–$K_2$ for response routines; MAXBAS for routing) were derived from literature-defined ranges. Model performance was assessed using objective functions (Kling-Gupta Efficiency, KGE; Coefficient of Determination, $R^2$) computed by HBV-Light, with KGE integrating correlation, bias, and variability components, and $R^2$ quantifying explained variance [9].

### *2.4.2 Parameter sensitivity analysis*

A Local Sensitivity Analysis (One-at-a-Time method) was conducted post-calibration to identify influential parameters. Using Monte Carlo simulations, parameters were individually perturbed within their predefined ranges, and changes in KGE and $R^2$ were evaluated. This approach highlighted parameters critical to calibration, prioritizing those with the strongest impact on streamflow simulation accuracy. While $R^2$ provided simplicity, its omission of bias assessment underscored the utility of KGE for holistic performance evaluation [9].

### *2.4.3 Calibration and validation*

Calibration is performed using GAP optimization, a method used to determine the optimal parameters based on the objective function values. In this study, the objective functions utilized are the Coefficient of Determination ($R^2$) and Kling-Gupta Efficiency (KGE). The equations used are as follows:

$$\mathrm{KGE}=1-\sqrt{(r-1)^2+(a-1)^2+(b-1)^2} \tag{7}$$

Where r is the correlation coefficient between observed and simulated values, α is the ratio of the standard deviation of simulations to observations, and b is the relative bias between simulations and observations [10].

$$R^2=\frac{\left[\Sigma_i\left(Q_{o,i}-\underline{Q}_o\right)\left(Q_{s,i}-\underline{Q}_s\right)\right]^2}{\Sigma_i\left(Q_{o,i}-\underline{Q}_o\right)^2\Sigma_i\left(Q_{s,i}-\underline{Q}_s\right)^2} \tag{8}$$

Where Qo is the observed streamflow, and Qs is the simulated streamflow.

**Table 4.** Performance Rating for $R^2$ and KGE

| Model Performance | $R^2$ | KGE |
|---|---|---|
| Very Good | 0.75 < R2 ≤ 1 | 0.9 ≤ KGE≤1 |
| Good | 0.65 < R2 ≤ 0.75 | 0.75≤KGE < 0.9 |
| Satisfactory | 0.50 < R2 ≤ 0.65 | 0.5 ≤ KGE < 0.75 |
| Unsatisfactory | KGE ≤ 0.5 | KGE < 0.5 |

The calibration process involves 10,000 iterations for global model runs, followed by 2,000 Powell local search iterations. A total of 10 populations is generated, with each population consisting of 1,000 parameter sets. If the results are unsatisfactory, recalibration is conducted by adjusting the parameter range based on previous calibration outcomes. This process continues iteratively until optimal parameters are obtained. Once calibration is complete, the best parameter set is selected for use in the model validation process. The model performance is then evaluated using the defined objective functions.

### 2.5 Uncertainty Analysis

Uncertainty arises when an event cannot be precisely described. When model outputs are compared with field observation data, the detected errors can be analyzed to determine where and why these errors occur [4]. Uncertainty analysis aims to estimate the potential range of variability expected from the model results. The results of hydrological models cannot be fully trusted or used without conducting an uncertainty analysis. A widely recognized framework classifies uncertainty sources into three categories: (1) parameter uncertainty, (2) model structural uncertainty, and (3) input data uncertainty.

The input data in hydrological models consist of hydrometeorological data and information on the physical conditions of a watershed. Despite technological advancements in data collection and processing, the data used in hydrological models remains incomplete, imprecise, and inherently uncertain, with uncertainty levels ranging from 10% to 40%. This uncertainty can lead to biased parameter estimations [3]. Several techniques have been developed to analyze uncertainty in input data, including Monte Carlo simulations, Bayesian statistics, and the Generalized Likelihood Uncertainty Estimation (GLUE) method [3].

Generalized Likelihood Uncertainty Estimation (GLUE) is an uncertainty analysis method is based on the equifinality paradigm, which rejects the notion of a single "optimal" parameter set. Instead, it is only possible to identify a population of parameter sets that can serve as good simulators within a hydrological modeling system. GLUE accommodates uncertainties across model inputs, parameters, and structure, making it a versatile tool for holistic uncertainty analysis [11].

# 3 Results and Discussion

## 3.1 Reference Model

The reference model or “golden standard” was developed as the primary benchmark for the uncertainty analysis. This model utilizes observed rainfall and discharge data, making it the most representative reference of the hydrological conditions in the study area. Initial calibration with default parameters optimized the HBV model’s alignment with observed hydrological dynamics. The calibration aims to adjust the model parameters so that the simulation results closely match the observed data, thereby producing an optimal hydrological representation.

Sensitivity analysis, evaluated via Kling-Gupta Efficiency (KGE) and $R^2$, identified parameters $K_0$ (baseflow recession coefficient) and MAXBAS (transformation function duration) as the most influential. MAXBAS exhibited pronounced sensitivity across both metrics, while $K_0$ showed significant variability in KGE. These highly sensitive parameters served as the basis for adjusting the parameter range in subsequent selection iterations, which were conducted three times until the optimal values were obtained (Table 5).

**Table 5.** Optimal parameter set

| Parameter | Value |
|---|---|
| **FC** | 1000 |
| **LP** | 1 |
| **Beta** | 1 |
| **Perc** | 6 |
| **UZL** | 35 |
| **K0** | 0,13 |
| **K1** | 0,15 |
| **K2** | 0,04 |
| **MAXBAS** | 1 |

The model simulation results were visualized in graphical form, comparing observed and simulated discharge during the calibration period (2013–2016) and validation period (2017–2018) (Figure 2). The graphs indicate that in both periods, the model successfully represented the observed discharge patterns. This is demonstrated by the alignment between simulated and observed discharge, reflecting the model’s strong performance in capturing the hydrological dynamics of the watershed. The model’s performance evaluation using KGE and $R^2$ metrics also confirmed its good performance in both periods, as detailed in Table 8.

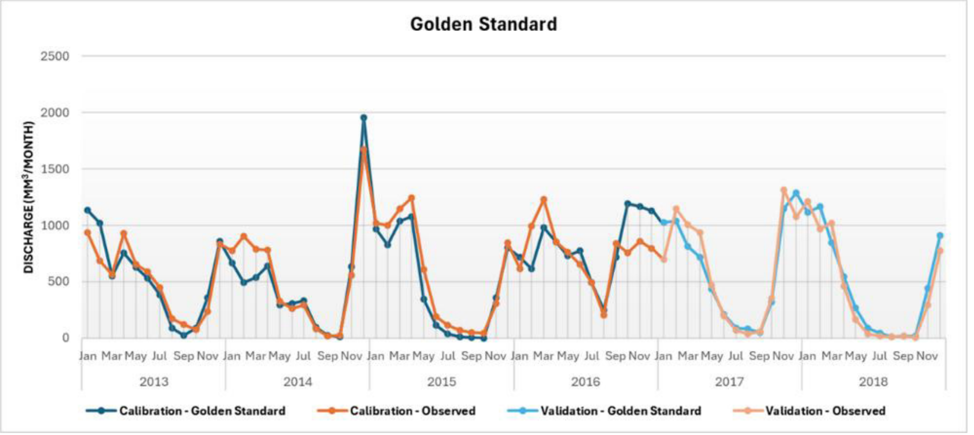


**Fig. 2.** Reference model discharge

**Table 6.** Description of satellite data used in this study

| Objective Function | Calibration | | Validation | |
|---|---|---|---|---|
| | Value | Performance | Value | Performance |
| **KGE** | 0,80 | Good | 0,80 | Good |
| **R2** | 0,64 | Good | 0,64 | Good |

## 3.2 Bias Correction

Satellite rainfall data obtained from Google Earth Engine underwent bias correction to minimize systematic deviations from ground-based observational data. The evaluation of bias for seven satellite rainfall products, before and after correction, was conducted using the Percent Bias (PBIAS) metric (Table 7). Prior to correction, all satellite datasets exhibited significant negative PBIAS values, indicating consistent underestimation compared to observational rainfall. The CPC and GSMaP datasets showed the largest biases, with PBIAS values of -40.54% and -33.76%, respectively.

**Table 7.** Bias-corrected satellite data using the quantile mapping method

| Objective Function | Satellite Rainfall | | | | | | |
|---|---|---|---|---|---|---|---|
| | CHIRPS | TRMM | GPM | PERSIANN | GSMAP | ERA5 LAND | CPC |
| **PBIAS** | -12.28 | -26.83 | -28.50 | -24.84 | -33.76 | -17.28 | -40.54 |
| | | | | | | | |
| **Objective Function** | **Corrected Satellite Rainfall** | | | | | | |
| | **CHIRPS** | **TRMM** | **GPM** | **PERSIANN** | **GSMAP** | **ERA5 LAND** | **CPC** |
| **PBIAS** | -0.38 | 1.37 | 2.69 | 0.60 | 0.09 | 1.78 | 0.16 |

Following bias correction, all satellite datasets demonstrated substantial improvements in PBIAS. The CPC dataset, which initially had the highest bias, achieved a near-neutral PBIAS of 0.16% post-correction. Similarly, GSMaP improved to a PBIAS of 0.09%, while CHIRPS retained a minor residual bias (-0.38%). Visual comparisons of rainfall distributions (Figures 3) confirmed that corrected satellite data aligned more closely with observational records.

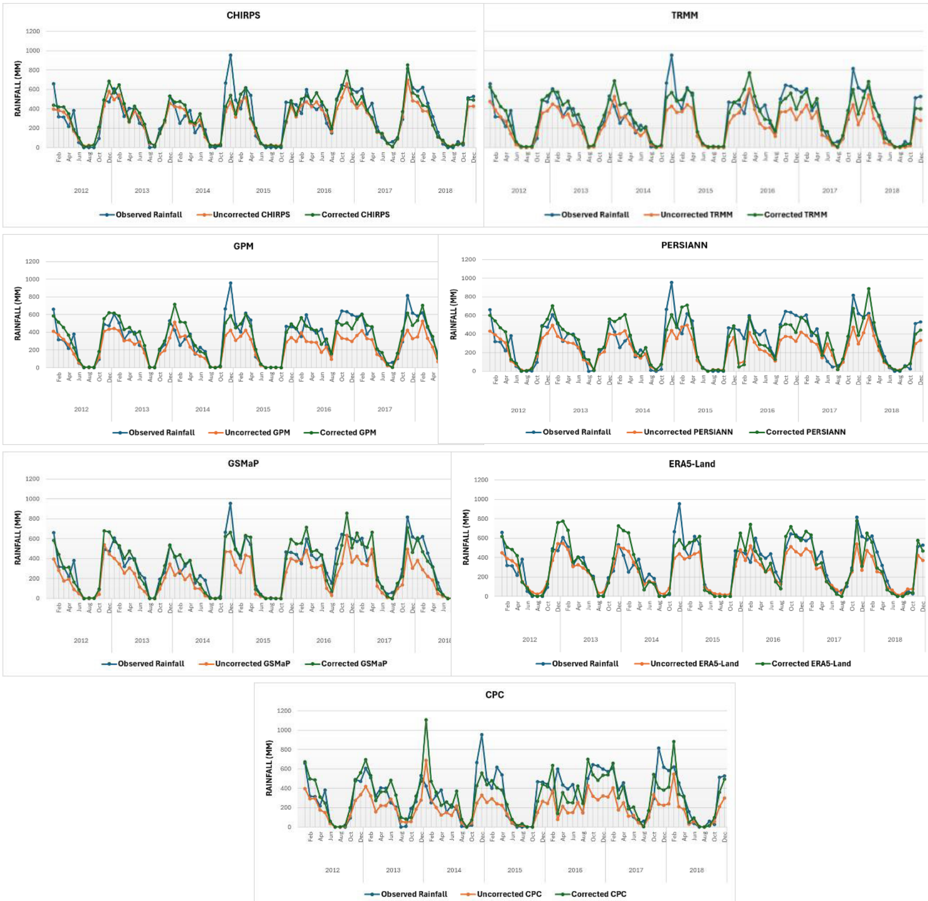


**Fig. 3.** Corrected and uncorrected satellite rainfall data comparison

To further evaluate the hydrological utility of the corrected datasets, hydrological simulations using the HBV model were conducted to evaluate the impact of corrections on streamflow predictions. Before bias correction, satellite rainfall inputs yielded variable model performance (Table 10). During the calibration period (2013–2016), $R^2$ values ranged from 0.18 (CPC) to 0.61 (TRMM and GPM), while KGE metrics were notably low, particularly for CPC (KGE = 0.09). In the validation period (2017–2018), most datasets exhibited performance degradation. For instance, PERSIANN's KGE declined from 0.35 (calibration) to 0.31 (validation), and CPC remained the poorest performer (KGE = 0.08), reflecting model instability with uncorrected inputs.

Bias correction significantly enhanced model performance across both calibration and validation periods (Table 8). During calibration, $R^2$ values stabilized or improved, with GSMaP achieving the highest $R^2$ (0.65). KGE improvements were particularly pronounced: GSMaP increased from 0.43 to 0.80, and CPC improved by 400% (0.09 to 0.45). Validation results confirmed sustained reliability, with GSMaP emerging as the top-performing dataset ($R^2$ = 0.65, KGE = 0.75). Notably, even CPC exhibited marked post-correction gains (KGE = 0.51),

**Table 8.** Corrected and uncorrected satellite rainfall data comparison

| **Objective Function** | **Uncorrected Satellite Rainfall** | | | | | | |
|---|---|---|---|---|---|---|---|
| | **CHIRPS** | **TRMM** | **GPM** | **PERSIANN** | **GSMAP** | **ERA5-LAND** | **CPC** |
| **Period** | **Calibration** | | | | | | |
| **R2** | 0.44 | 0.61 | 0.61 | 0.45 | 0.58 | 0.48 | 0.18 |
| **KGE** | 0.55 | 0.50 | 0.40 | 0.35 | 0.43 | 0.52 | 0.09 |
| **Period** | **Validation** | | | | | | |
| **R2** | 0.58 | 0.52 | 0.59 | 0.44 | 0.59 | 0.61 | 0.27 |
| **KGE** | 0.51 | 0.33 | 0.36 | 0.35 | 0.31 | 0.39 | 0.08 |

| **Objective Function** | **Corrected Satellite Rainfall** | | | | | | |
|---|---|---|---|---|---|---|---|
| | **CHIRPS** | **TRMM** | **GPM** | **PERSIANN** | **GSMAP** | **ERA5-LAND** | **CPC** |
| **Period** | **Calibration** | | | | | | |
| **R2** | 0.41 | 0.63 | 0.63 | 0.44 | 0.65 | 0.44 | 0.21 |
| **KGE** | 0.64 | 0.79 | 0.77 | 0.65 | 0.80 | 0.62 | 0.45 |
| **Period** | **Validation** | | | | | | |
| **R2** | 0.55 | 0.57 | 0.65 | 0.42 | 0.65 | 0.56 | 0.30 |
| **KGE** | 0.66 | 0.65 | 0.73 | 0.63 | 0.75 | 0.70 | 0.51 |

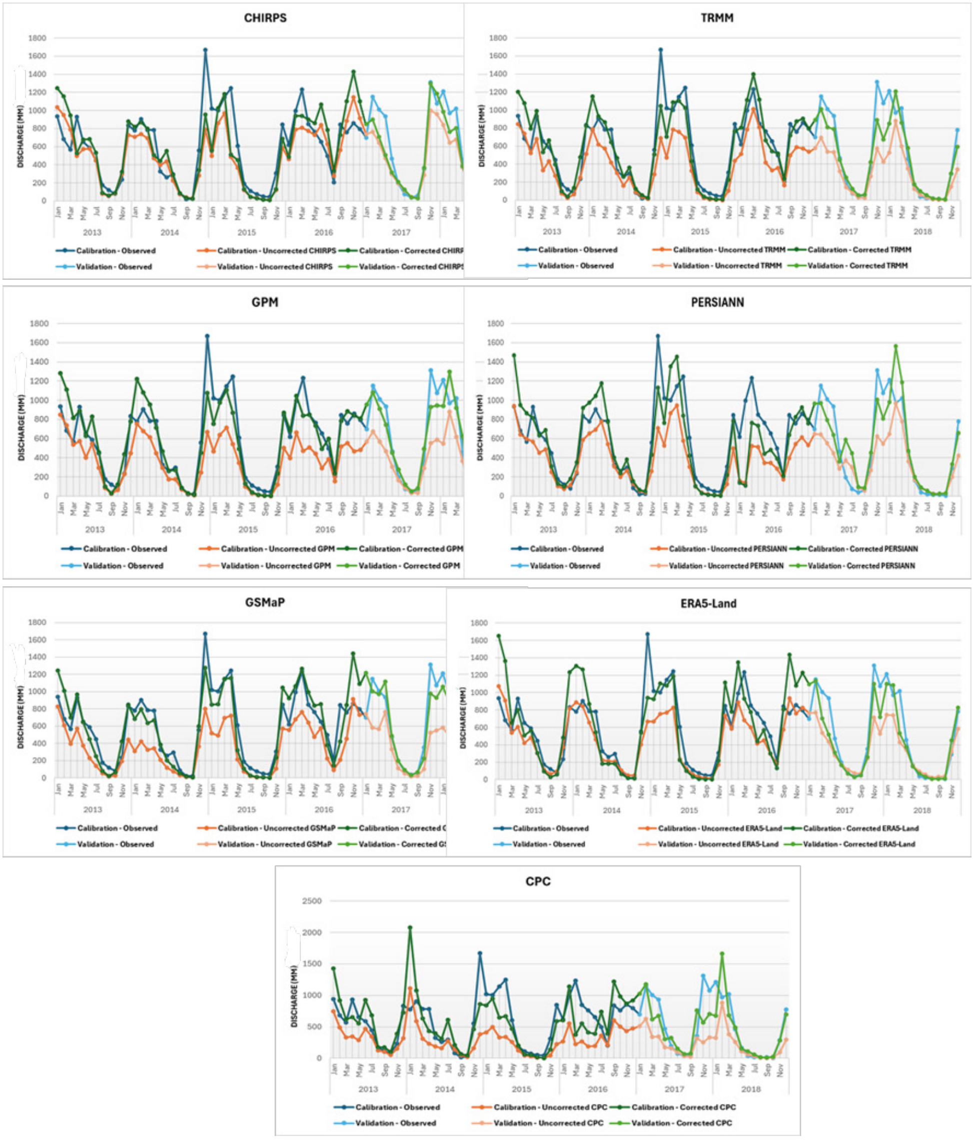


**Fig. 4.** Discharge comparison of corrected and uncorrected satellite rainfall data after running in the HBV model

### 3.3 Uncertainty Analysis

The uncertainty analysis framework involved hydrological simulations using multiple satellite rainfall datasets across calibration (2013–2016) and validation (2017–2018) periods. Model outputs (simulated discharge and objective function values) were generated via HBV Light, enabling rapid performance evaluation. A likelihood threshold (KGE ≥ 0.6, was applied to filter behavioral parameter sets. Six of seven satellite datasets met this criterion (Table 9) and were retained for uncertainty quantification.

**Table 9.** Likelihood sampling results based on threshold

| Data Satelite | Likelihood (KGE) | |
|---|---|---|
| | Calibration | Validation |
| **CPC** | 0.45 | 0.51 |
| **ERA5-LAND** | 0.62 | 0.63 |
| **CHIRPS** | 0.64 | 0.65 |
| **PERSIANN** | 0.65 | 0.66 |
| **GPM** | 0.77 | 0.70 |
| **TRMM** | 0.79 | 0.73 |
| **GSMaP** | 0.80 | 0.75 |

Uncertainty bounds, derived from these datasets, were visualized as simulation ranges alongside observed discharge (Figure 5). The median of the uncertainty range was used as a robust central tendency measure due to non-normal discharge distributions. During calibration, narrow uncertainty ranges dominated low-flow periods (e.g., 63% of observed data fell within bounds), reflecting reliable model performance under typical conditions. However, extreme events (e.g., early 2014, late 2016) exhibited wider bounds, with median simulations overestimating observed peaks. Conversely, satellite inputs failed to capture a significant rainfall event in early 2015, producing underestimates despite low uncertainty ranges, likely due to dataset limitations in resolving localized extremes.

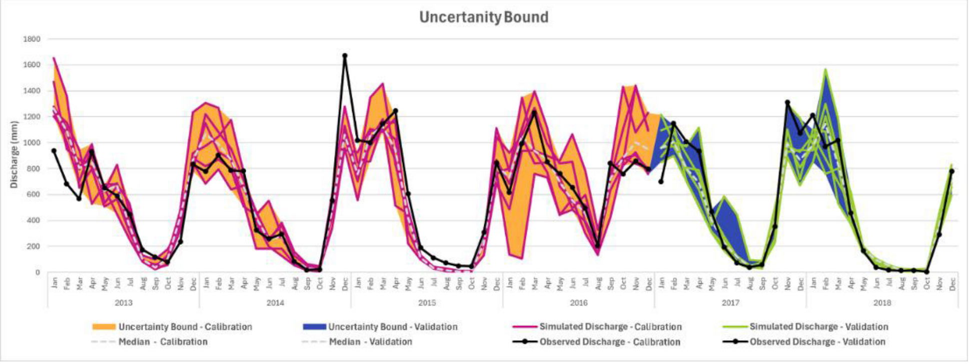


**Fig. 5.** Uncertainty analysis results on satellite rainfall data

Table 12 presents the results of the uncertainty analysis obtained from six satellite-based rainfall input datasets, which define the range of uncertainty. The analysis results indicate that during the calibration period, 63% of the observed discharge data fell within the uncertainty range, while during the validation period, this value slightly increased to 64%. Although this coverage percentage includes a significant portion of the observed discharge data, the results are relatively unsatisfactory because the figure is still far from the expected reliability of satellite data as an alternative input for hydrological models when observational data from stations are unavailable. This coverage percentage indicates that the satellite data used has not yet fully represented the observed discharge data.

**Table 10.** Position of observed discharge within the uncertainty range

| Discharge Within Uncertainty Bound | Calibration (Month) | Validation (Month) |
|---|---|---|
| **Inside** | 32 | 16 |
| **Outside** | 19 | 9 |
| **% Inside** | **0.63** | **0.64** |

To identify the most representative datasets, median uncertainty ranges were compared to observed discharge using KGE (Table 11). GPM outperformed others in calibration (KGE = 0.98), followed by TRMM (KGE = 0.95) and CHIRPS (KGE = 0.90). TRMM and PERSIANN maintained stable performance in validation, while ERA5-Land ranked lowest (KGE = 0.78). Based on these results, the GPM and TRMM datasets are considered the most representative of satellite input data uncertainty.

**Table 11.** Relationship Between the Median of Satellite Data Input Uncertainty Range and Simulated Discharge

| Calibration | | | | | | |
|---|---|---|---|---|---|---|
| **Objective Function** | **CHIRPS** | **TRMM** | **GPM** | **PERSIANN** | **GSMAP** | **ERA5-LAND** |
| **KGE** | 0.90 | 0.95 | 0.98 | 0.86 | 0.87 | 0.78 |

| Validation | | | | | | |
|---|---|---|---|---|---|---|
| **Objective Function** | **CHIRPS** | **TRMM** | **GPM** | **PERSIANN** | **GSMAP** | **ERA5-LAND** |
| **KGE** | 0.93 | 0.95 | 0.92 | 0.86 | 0.90 | 0.91 |

### 3.4 Discussion

During the data preparation process, temporal resolution adjustments were applied to all datasets. Adjusting the temporal resolution of satellite-based rainfall data is a crucial step to ensure compatibility with the HBV hydrological model's input requirements. Through spatial analysis using the Thiessen Polygon method, the spatial distribution of rainfall can be accurately represented via a weighted average based on the influence area of each station. This approach enhances the quality of input data and the reliability of the model in representing rainfall conditions in the Upper Bogowonto Watershed.

The impact of climate change is one of the key factors in analyzing temperature variability and potential evapotranspiration. The increasing trend of potential evapotranspiration since mid-2016 and extreme daily temperature fluctuations indicate a significant influence of climate change on local climate conditions. The climate change also leads to increased rainfall intensity and discharge, despite a declining trend in the number of rainy days. This suggests that climate change affects not only rainfall but also other climatic parameters that influence hydrological processes. This analysis highlights the importance of considering climate change impacts in hydrological models to improve prediction reliability.

The use of elevation zones in the HBV model is one of the steps to enhance simulation accuracy. Considering temperature and rainfall variability based on elevation allows for a more accurate representation of the spatial distribution of climatic parameters. The steep topography of the Upper Bogowonto Watershed necessitates this approach to ensure the model produces reliable discharge simulations. The temperature lapse rate and rainfall gradient based on elevation, established through the calibration process, align with the geographical conditions of the study area.

### *3.4.1 Reference model result*

Sensitivity analysis results indicate that the K0 and MAXBAS parameters exhibit high sensitivity, meaning that small changes in these parameters can significantly impact model performance. This sensitivity underscores the importance of selecting an appropriate parameter range to ensure optimal representation in the hydrological model. MAXBAS, which exhibits high sensitivity in both KGE and $R^2$ metrics, reflects the critical role of this parameter in controlling the flow response time in the HBV model. MAXBAS is a routing parameter that controls the hydrograph shape by delaying flow. The optimal MAXBAS value of 1 results in a sharp and rapid hydrograph, indicating that the study area experiences a fast-flowing hydrological response. This aligns with the steep topography of the Upper Bogowonto Watershed, making the MAXBAS parameter more sensitive

Although the model demonstrates good overall performance, its limitations in representing peak flow remain a primary concern. The model often underestimates peak discharge, indicating that it is less reliable in capturing extreme events. This may be due to several factors, including model parameter uncertainty, hydrological data quality, climate variability, complex topography, and human activities. Previous studies have also reported similar challenges, where hydrological models struggle to produce accurate simulations for peak discharge [12]. The limitations in representing peak discharge suggest that the model is more suitable for long-term hydrological analysis rather than applications requiring high-precision predictions of extreme events, such as flood forecasting. Additionally, the impact of climate change on flow variability should be considered to develop more reliable hydrological models in the future.

### *3.4.2 Bias correction of satellite rainfall data*

Bias correction results indicate that the quantile mapping method is effective in improving the distribution of satellite-based rainfall data, making it more consistent with observational data. The significant improvement in PBIAS values suggests that systematic bias can be drastically reduced, particularly in datasets with high initial bias, such as CPC and GSMaP. These results emphasize the importance of bias correction in enhancing the quality of satellite data.

Analysis using the HBV hydrological model reveals that improvements in $R^2$ and KGE values after bias correction demonstrate the capability of corrected satellite data to more accurately represent discharge patterns. Bias correction not only reduces systematic errors in the data but also improves the alignment between satellite data and hydrological patterns in the watershed. It is noteworthy that some datasets performed better during the validation period compared to the calibration period, which may be due to greater consistency in the validation dataset.

The finding that satellite data with higher temporal resolution, such as GSMaP, TRMM, and GPM, result in better model performance suggests that temporal resolution plays a critical role in improving hydrological model accuracy. This is consistent with the study by [13], which found that temporal resolution is more significant than spatial resolution in enhancing hydrological model performance.

Overall, bias correction is a crucial step in utilizing satellite data for hydrological analysis, as these data serve as a primary factor influencing hydrological components within a watershed. Changes in precipitation values can alter water balance and model efficiency coefficients. Bias correction improves data quality, thereby enhancing model accuracy in representing hydrological patterns, although it remains insufficient in improving extreme discharge representation.

#### *3.4.3 Uncertainty analysis*

The analysis results confirm that the Generalized Likelihood Uncertainty Estimation (GLUE) method is effective in identifying the uncertainty of satellite-based rainfall input in hydrological models. This method employs a likelihood-based threshold approach using KGE values to determine feasible solutions for analysis. However, several limitations must be considered. One limitation is the restricted number of datasets. Of the seven tested rainfall datasets, only six were deemed suitable. This results in a relatively narrow uncertainty range, which limits the model's ability to fully represent observed discharge data. Additionally, other factors such as precipitation process complexity, rainfall data collection techniques, and difficulties in measuring light rainfall contribute to simulation uncertainties [14].

Another drawback of the GLUE method is the subjectivity involved in selecting the likelihood threshold. Setting the threshold too high results in a more robust approach but narrows the uncertainty range, whereas setting it too low produces an overly broad uncertainty range, reducing accuracy in uncertainty representation. This aligns with the findings of [15], who stated that the confidence interval in GLUE does not represent a statistical confidence interval but rather model uncertainty. Unlike statistical confidence intervals, which estimate the true population parameter with a certain confidence level, the confidence interval in GLUE is derived from the model output distribution and does not guarantee that a 90% confidence interval will encompass 90% of true values.

[15], proposed an empirical approach to adjust uncertainty bounds to match the desired coverage level by modifying the number of feasible datasets. This ensures that the uncertainty interval more realistically represents observed data, although it remains non-statistical. In this study, the tested dataset population consisted of only seven datasets, making confidence interval estimation impractical. The limited number of solutions was deemed insufficient for accurately representing uncertainty, leading to the adoption of a direct evaluation approach without confidence intervals.

The model's limited ability to capture peak discharge, particularly during the validation period, indicates decreased accuracy under extreme climate conditions. Additionally, the physical complexity of the watershed, such as topographic variation and watershed shape, also affects discharge simulation accuracy. Nonetheless, this study demonstrates that the GSMaP datasets provide the best performance in satellite-based input uncertainty analysis. This reinforces the idea that higher temporal resolution in satellite data improves hydrological simulation quality.

Overall, the GLUE approach has successfully provided valuable insights into hydrological model uncertainty, although there is room for improvement. The use of satellite data as an alternative input for hydrological models remains highly promising, particularly if satellite data accuracy in capturing rainfall variability under diverse climate conditions is enhanced.

## 4 Conclusions

The GLUE method successfully evaluated the uncertainty of satellite-based rainfall data in the HBV hydrological model. Among the seven datasets tested, GSMaP outperformed the others, demonstrating high accuracy and stability with $R^2$ values of 0.65 and KGE values of 0.80 during calibration, and $R^2$ values of 0.65 and KGE values of 0.75 during validation. GSMaP also exhibited strong performance in capturing the variability of observed discharge, particularly during peak flows, which other datasets struggled to replicate. Although the uncertainty ranges were narrower during low flows and wider during peak flows, GSMaP consistently performed well, achieving KGE values of 0.87 in calibration and 0.90 in validation. These results highlight GSMaP as the most reliable dataset for hydrological modeling in the Upper Bogowonto Watershed. However, further improvements in uncertainty estimation are needed to enhance the reliability of hydrological predictions, especially under extreme conditions. Future research should focus on refining the uncertainty framework to better support decision-making in water resource management.

## References

1. C. Asdak and U. G. M. Press, Hidrologi dan Pengelolaan Daerah Aliran Sungai. (UGM PRESS, 2023)
2. S. Bergström, "THE HBV model - its structure and applications," Swedish Meteorol. Hydrol. Institute, Norrköping. **4**, 4, 1–3, (1992)
3. E. Moges, Y. Demissie, L. Larsen, and F. Yassin, "Review: Sources of hydrological model uncertainties and advances in their analysis," Water (Switzerland). **13**, 1, 1–23 (2021) https://doi: 10.3390/w13010028
4. V. P. Singh, R. Singh, P. K. Paul, D. S. Bisht, and S. Gaur, Hydrological Processes Modelling and Data Analysis. (Springer Singapore, 2024). https://doi.org/10.1007/978-981-97-1316-5
5. J. Fu, N. Xia, and G. Zhang, "Research on Landform Classification of Beijing-Tianjin-Hebei Region Based on SRTM Remote Sensing Image Data," *I*OP Conf. Ser. Earth Environ. Sci. **252**, 5 (2019) https://doi.org/10.1088/1755-1315/252/5/052006.
6. S. Trajkovic, "Hargreaves versus Penman-Monteith," J. Irrig. Drain. Eng. **133**, 1, 38–42 (2007)
7. D. Maraun, "Bias correction, quantile mapping, and downscaling: Revisiting the inflation issue," J. Clim. **26**, 6, 2137–2143 (2013) https://doi.org/10.1175/JCLI-D-12-00821.1.
8. D. N. Moriasi, J. G. Arnold, M. W. Van Liew, R. L. Bingner, R. D. Harmel, and T. L. Veith, "Model Evaluation Guidelines for Systematic Quantification of Accuracy in Watershed Simulations," **50**, 3, 885–900 (2007) https://doi.org/10.13031/2013.23153.
9. C. Onyutha, "Pros and cons of various efficiency criteria for hydrological model performance evaluation," *Proc. Int. Assoc.* Hydrol. Sci. **385**, 181–187 (2024) https://doi.org/10.5194/piahs-385-181-2024.
10. H. V. Gupta, H. Kling, K. K. Yilmaz, and G. F. Martinez, "Decomposition of the mean squared error and NSE performance criteria: Implications for improving hydrological modelling," J. Hydrol. **377**, 1–2, 80–91 (2009) https://doi.org/10.1016/j.jhydrol.2009.08.003.
11. G. Tegegne, Y. O. Kim, S. B. Seo, and Y. Kim, "Hydrological modelling uncertainty analysis for different flow quantiles: a case study in two hydro-geographically different watersheds," Hydrol. Sci. J. **64**, 4, 473–489 (2019) https://doi.org/10.1080/02626667.2019.1587562.
12. S. Bhattarai, Y. Zhou, N. M. Shakya, and C. Zhao, "Hydrological modelling and climate change impact assessment using HBV light model: A case study of Narayani river basin, Nepal," Nat. Environ. Pollut. Technol. **17**, 3, 691–702 (2018)
13. Q. Zhu, X. Qin, D. Zhou, T. Yang, and X. Song, "Impacts of spatiotemporal resolutions of precipitation on flood event simulation based on multimodel structures -- a case study

over the Xiang River basin in China," Hydrol. Earth Syst. Sci. **28**, 7, 1665–1686 (2024) https://doi.org/10.5194/hess-28-1665-2024.

14. J. Gou, C. Miao, S. Sorooshian, Q. Duan, X. Guo, and T. Su, "Satellite-based precipitation error propagation in the hydrological modeling chain across China," J. Hydrol. **632**, November 2023, 130906 (2024) https://doi.org/10.1016/j.jhydrol.2024.130906.
15. R.-S. Blasone, J. A. Vrugt, H. Madsen, D. Rosbjerg, B. A. Robinson, and G. A. Zyvoloski, "Generalized likelihood uncertainty estimation (GLUE) using adaptive Markov Chain Monte Carlo sampling," Adv. Water Resour.**31**, 4, 630–648 (2008) https://doi.org/10.1016/j.advwatres.2007.12.003.